Applied Catalysis B: Environmental 331 (2023) 122696

Contents lists available at ScienceDirect

Applied Catalysis B: Environmental

journal homepage: www.elsevier.com/locate/apcatb

Boosting simultaneous catalytic removal of NO_x and toluene via cooperation of Lewis acid and oxygen vacancies

Lyumeng Ye [a,b,c,d], Peng Lu [a,c,d], Yan Xianhui [a,c,d], Haibao Huang [b,*]

[a] South China Institute of Environmental Sciences, MEE, 510655 Guangzhou, PR China
[b] School of Environmental Science and Engineering, Sun Yat-sen University, 510275 Guangzhou, PR China
[c] Guangdong Province Engineering Laboratory for Air Pollution Control, Guangzhou 510655, PR China
[d] Guangdong Provincial Key Laboratory of Water and Air Pollution Control, Guangzhou 510655, PR China

ARTICLE INFO

Keywords:
NH_3-SCR
Toluene oxidation
MnCe/TNT
Lewis acid
Oxygen vacancies

ABSTRACT

MnO_x-CeO_2 supported on TiO_2 nanotube (MnCe/TNT) were purposely tailored to concurrently lower toluene oxidation temperature and keep high N_2 selectivity during simultaneous removal of NO_x and toluene via low-temperature NH_3-SCR ($\leq$ 300 °C). Over 80% NO and toluene conversions were simultaneously achieved within 182–300 °C with N_2 selectivity of more than 90%. Strong Lewis acidity and plentiful oxygen vacancies were synchronously generated as Mn^{3+} + Ce^{4+} shifted to Mn^{4+} + Ce^{3+}, and this shift was enhanced by the TiO_2 nanotube. Lewis acid and oxygen vacancies synergistically facilitated NH_3-SCR and accelerated toluene adsorption/activation and ring opening, thus dramatically lowering toluene conversion temperature to match that of NH_3-SCR. Gaseous NO_x predominantly reacted with NH_3 adsorbed on Lewis acid sites, following the Eley-Rideal mechanism to form N_2. The consumption of adsorbed oxygen via toluene decomposition significantly suppressed the unfavorable catalytic NH_3 oxidation and N_2O formation, contributing to the high N_2 selectivity.

1. Introduction

In order to mitigate the increasing trend of ozone (O_3) and aerosol pollution, the Chinese government declared that the control of NO_x and VOCs was an urgent demand during the 14th Five-Year Plan period. Industrial furnaces are one of the dominant sources of both NO_x and VOCs. Taking the advantage of widely used selective catalytic reduction with ammonia (NH_3-SCR) technology, the SCR catalysts can simultaneously catalyze NO_x reduction into N_2 and oxidize VOCs into CO_2 in one unit [1,2]. This strategy has gained increasing interests due to its simplicity and cost-effectiveness. However, the reducibility of current well-known SCR catalysts is not appropriate to activate VOCs oxidation at low temperature to match the temperature window of NH_3-SCR [3,4]. Therefore, it is highly necessary to lower VOC conversion temperature to simultaneously achieve efficient NO reduction and VOC oxidation.

Toluene, as a typical VOC and major contributor to the O_3 and aerosol formation [5,6], is abundantly discharged along with NO_x from many processes such as biomass combustion and solid waste incineration [7,8]. The actual exhaust temperatures from biomass combustion and solid waste incineration are always below 300 °C. The simultaneous removal of NO_x and toluene via low-temperature SCR (denoted as DeNO_xTL, $\leq$300 °C) is highly necessary while it has not received enough attention and research yet. Unlike widely-studied simultaneous removal of NO_x and chlorinated VOCs, Lewis and Brønsted acid sites are not the requirements for toluene oxidation since no C–Cl bond needs to be broken in the molecular structure of toluene. Nevertheless, it has been proved that oxygen vacancies are conducive to oxygen species activation and mobility, thus resulting in a significant improvement in toluene catalytic oxidation [9]. Numerous efforts have been carried out for the enhancement of low-temperature reducibility and the introduction of oxygen vacancies to improve toluene catalytic oxidation and lower the conversion temperature. For example, Liao's groups [10–12] indicated that transition metal (Cu, Ce and Fe) modification over V-W/Ti type catalysts could improve the redox equilibrium and increase oxygen vacancies, leading to a better DeNO_xTL activity. The introduction of Al_2O_3 facilitated the reducibility of CuO-CeO_2 and induced oxygen vacancies, thus contributing to 90% of NO and toluene conversion within 235–300 °C [13]. The introduction of MnO_x into CuAl catalysts also improved reducibility and oxygen vacancies generation, which significantly lower the 80% toluene conversion temperature from 315 to 250 °C [14]. In our previous study, it was demonstrated that the DeNO_xTL process over MnO_x-CeO_2 was practicable with the operating

* Corresponding author.
E-mail address: seabao8@gmail.com (H. Huang).

https://doi.org/10.1016/j.apcatb.2023.122696
Received 30 January 2023; Received in revised form 20 March 2023; Accepted 25 March 2023
Available online 27 March 2023

temperature windows over 100 °C, which could be ascribed to abundant oxygen vacancies and better low-temperature reducibility [15]. However, it is noteworthy that the superior reactivity and mobility of oxygen species as well as the strong reducibility of catalysts would obviously result in the formation of abundant greenhouse gas N_2O and poor N_2 selectivity of NH_3-SCR. Therefore, it still presents a big challenge for the practical application of De*NO$_x$TL* process to concurrently lower toluene conversion temperature and keep high N_2 selectivity.

It is well known that Lewis acid sites are crucial to the low-temperature NH_3-SCR activity and selectivity [16], while its importance is not well addressed for catalytic VOCs oxidation. In principle, catalytic VOCs oxidation follows the Mars and van Krevelen (MvK) mechanism, which generally consists of three steps, including (i) VOC molecule activation on metal cations; (ii) VOC molecule oxidation by lattice oxygen; and (iii) metal cations circulation and O_2 re-oxidation [17]. Only few studies have realized the contribution of the surface Lewis acid sites in the (i) step, in which the metal cations would act as Lewis acid sites. Yuan et al. [18] discovered that a main bonding was created between surface Lewis acid sites and HCHO, resulting in HCHO strong chemisorption and activation. Yang et al. [19] confirmed that Lewis acid could enable C−H bond dissociation and therefore enhanced catalytic methane combustion. It is deduced that the regulation of Lewis acid sites of catalysts could be an effective strategy to lower VOC oxidation temperature. Therefore, the efficient toluene degradation and suppression of N_2O formation can be concurrently expected via improving Lewis acid sites of catalyst without increasing its redox capacity.

Titania nanotube (TNT) would yield a stronger Lewis acid strength as well as more Lewis acid sites after ethanol treatment [20,21]. Combining the best properties of MnO_x-CeO_2 related to abundant oxygen vacancies and TNT properties associated with large specific surface area and plentiful Lewis acid sites, MnCe/TNT catalysts were purposely tailored to enhance the performance of simultaneous catalytic removal of NO_x and toluene. The key structural properties of MnCe/TNT were systematically studied, and the function of Lewis acid sites and oxygen vacancies in NH_3-SCR and toluene degradation were intensively investigated. A comprehensive analysis of the intermediates during the De*NO$_x$TL* process was carried out via *in situ* DRIFT and PTR-ToF-MS. As a result, the De*NO$_x$TL* performance was greatly boosted by the cooperation of Lewis acid sites and oxygen vacancies, and the mechanism was proposed.

2. Experimental section

2.1. Catalyst synthesis

The synthesis of the titania nanotubes (TNT) in this study was achieved by the hydrothermal method and then with ethanol treatment. Commercial TiO_2 (P25, Degussa AEROSIL) was used as the precursor. Detailed preparation was shown in Supporting Information (SI).

The $Mn_xCe_{1-x}O_2$/TNT catalysts with 20 wt.% loading of metals on the TNT were prepared by wet impregnation method. $Ce(NO_3)_3{\cdot}6H_2O$ and 50 wt.% $Mn(NO_3)_2$ used as the metal oxide precursors. The resultant products were denoted as $Mn_xCe_{1-x}O_2$/TNT, with x molar values of 1, 0.9, 0.8, 0.5 and 0. The mixture solution was stirred for 5 h, then dried at 105 °C, and calcined at 450 °C for 3 h in air. For comparison, the $Mn_xCe_{1-x}O_2/TiO_2$ catalyst was prepared by the same wet impregnation method using pristine P25 as the supports, and the $Mn_xCe_{1-x}O_2$ catalyst was synthesized using a conventional coprecipitation method. The preparation details of all catalysts can be found in SI.

2.2. Activity measurements

The catalytic De*NO$_x$TL* was carried out in a fixed-bed quartz reactor (i.d. = 8 mm) using 0.2 g sample (40−60 meshes). The reaction feed consisted of 500 ppm NH_3, 500 ppm NO, 50 ppm toluene, 10 vol.% O_2, 5 or 10 vol.% H_2O (when used), and balanced with N_2. The gas hourly space velocity (GHSV) was 60, 000 mL/(g·h). The inlet and outlet gas concentrations were analyzed on-line by a FTIR (GASMET DX-4000). A more detailed description of the catalytic activity measurements was offered in SI.

2.3. Characterizations

The detailed information of XRD, BET, H_2-TPR, XPS, EPR, Raman, HR-TEM, Py-IR, TPD, *in situ* or *operando*-DRIFTs, TD-GC-MS and PTR-ToF-MS were given in SI.

3. Results and discussion

3.1. Catalytic performances of NO and toluene removal

Toluene and NO conversions of $Mn_xCe_{1-x}O_2$/TNT catalysts with different Mn/Ce molar ratios were investigated. Among them, the $Mn_{0.9}Ce_{0.1}O_2$/TNT displayed the best catalytic performance (Fig. S1). Toluene oxidation was notably promoted over $Mn_{0.9}Ce_{0.1}O_2$/TNT at low temperature with T_{90} = 196 °C (90% of toluene conversion), which was much better than most of Mn-based catalysts reported in literatures [22]. More importantly, the $Mn_{0.9}Ce_{0.1}O_2$/TNT exhibited a very broad active temperature window of 182–300 °C at which both NO and toluene conversions exceeded 80% (Table S1). In this temperature range, the N_2 selectivity of the $Mn_{0.9}Ce_{0.1}O_2$/TNT could keep over 90%. Thus, $Mn_{0.9}Ce_{0.1}O_2$/TNT was selected for further experiments. For comparison, both $Mn_{0.9}Ce_{0.1}O_2$ and $Mn_{0.9}Ce_{0.1}O_2/TiO_2$ showed a narrow temperature window of ~232–300 °C and a sharp decline of N_2 selectivity to less than 60% (Fig. 1). $Mn_{0.9}Ce_{0.1}O_2$/TNT assigned as MnCe/TNT, $Mn_{0.9}Ce_{0.1}O_2/TiO_2$ assigned as MnCe/TiO_2, and $Mn_{0.9}Ce_{0.1}O_2$ assigned as MnCe hereafter, respectively.

In the De*NO$_x$TL* process, the SCR feed gas imposed little impact on toluene conversion while improving toluene mineralization over MnCe/TNT. Compared with the NH_3-SCR process, the introduction of toluene caused a slight decrease of less than 5% in De*NO$_x$* activity. Interestingly, the N_2 selectivity was almost not sensitive to toluene addition, it maintained above 90% when the temperature was below 300 °C (Fig. 2). Due to the competitive adsorption and dynamic diameter of NH_3, NO_x and toluene, a considerable decrease of the De*NO$_x$TL* activity and selectivity frequently occurred at low temperature (<300 °C) [15]. However, over MnCe/TNT, high NO and toluene conversions were maintained with high N_2 selectivity and mineralization. Thus, it can be said that NH_3-SCR and toluene oxidation displayed a synergistic enhancement to some extent.

The working conditions over MnCe/TNT were tested and found that NO conversion of ~80% and toluene conversion of ~100% could maintain under 5 or 10 vol.% H_2O conditions within 250–300 °C (Fig. 2 and Fig. S2). The excellent hydrothermal stability met the requirements of the De*NO$_x$TL* process in practical application. However, SO_2 poisoning still occurred by the formation of NH_4HSO_4 (ABS) on active sites. A more rapid deactivation process was observed under 250 ppm SO_2 and 10 vol.% H_2O condition (Fig. S3). These results indicated that MnCe/TNT was suitable for the De*NO$_x$TL* process in wet flue gas with low-concentration SO_2 from solid waste incineration and biomass burning [23–25].

3.2. Basic physicochemical properties

The XRD patterns illustrated that the MnCe/TNT exhibited MnO_2 patterns (PDF #81–2261) (Fig. S4). The TEM analysis indicated that the addition of Mn and Ce did not change the tubular structure of TNT, and a few isolated nanoparticles were observed inside the hollow channels of the MnCe/TNT (Fig. 3). In the HRTEM image, it was difficult to search for sharp lattice fringes of the nanoparticles inside the tubular structure of TNT, deduced that MnCe solid solution was generated, resulting in

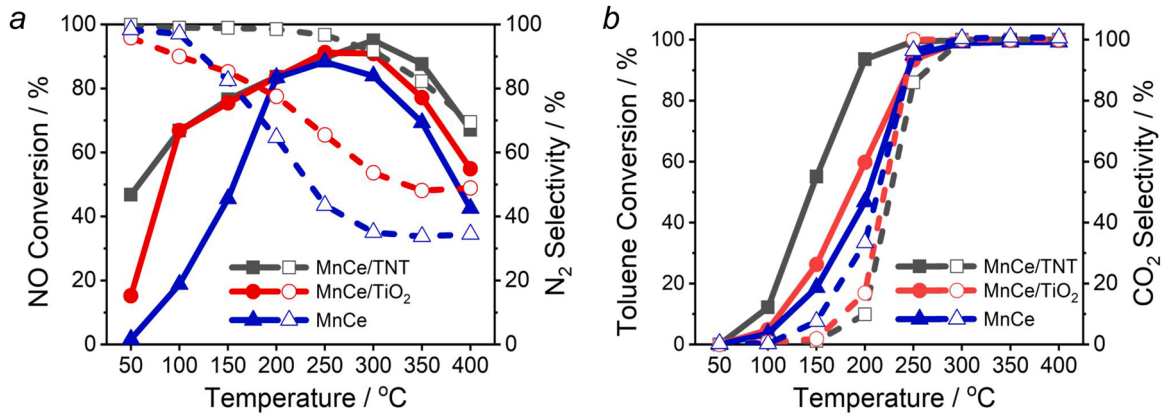

Fig. 1. (a) NO conversion (solid line) and N_2 selectivity (dash line), (b) toluene conversion (solid line) and CO_2 selectivity (dash line).

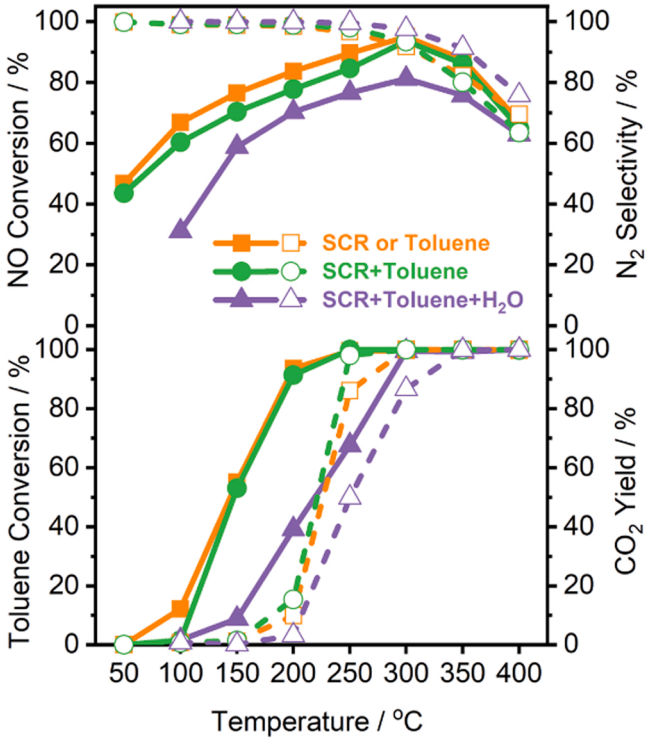

Fig. 2. NO conversion (solid line), N_2 selectivity (dash line), toluene conversion (solid line) and CO_2 selectivity (dash line) over MnCe/TNT catalyst. Reaction conditions: $[NH_3]$ = [NO] = 500 ppm, [Toluene] = 50 ppm, $[H_2O]$ = 10 vol.% (when used), O_2 = 10 vol.%, N_2 as the balance gas, GHSV = 60,000 mL/(g·h).

crystal disorder and lattice defects [26,27]. The TEM-mapping images further confirmed that active Mn and Ce were highly dispersed within TNT. The inner diameter and length of the MnCe/TNT were 8–10 nm and several hundred nanometers, respectively. TNT contributed to S_{BET} enhancement of MnCe/TNT compared with MnCe/TiO_2 and MnCe (Table S2).

When MnCe was coupled with TNT, the Ce^{3+}/Ce (Fig. 4(a)) and Mn^{4+}/Mn^{3+} (Fig. 4(b)) ratios were increased from 26.4% to 29.6% and from 43.3% to 52.4%, respectively (Table S3). Ce^{3+} and Mn^{4+} cations mainly exist in the states of Ce_2O_3 and MnO_2, respectively. It was reported that the conduction band energies (E_c) *vs* standard hydrogen electrode of Ce_2O_3 and MnO_2 were − 0.5 eV and 1.33 eV, respectively [28]. Therefore, MnO_2 with more positive E_c would prefer to get electrons from Ce_2O_3, resulting in the lack of electrons within Ce_2O_3. The electrophilicity of Ce_2O_3 had been confirmed to enhance the Lewis acidity [28]. NH_3-TPD profiles illustrated that the NH_3 adsorption capacity of MnCe/TNT was much higher than those of MnCe and MnCe/TiO_2 (Fig. S5). The Py-IR was used to identify the types of acidity (Fig. 5(a)). The peaks at 1446 cm^{-1}, 1540 cm^{-1}, and 1491 cm^{-1} were assigned to the Lewis–coordinated pyridine (L), Brønsted–coordinated pyridine (B), and Lewis + Brønsted–coordinated pyridine (L + B), respectively [29]. The results showed that MnCe/TNT exhibited much stronger Lewis acidity but fewer Brønsted acid sites than other samples (Table S3). The ethanol treatment on TNT would result in a remarkable increase of structural ion-exchangeable OH groups. Ti atoms of TNT and OH groups would be combined with each other by linear Ti–OH and bridged Ti–OH [20]. When MnCe/TNT was prepared, the addition of Mn^{2+} ions would exchange with the protons of Ti–OH, forming Mn $(OH)^+$ species that were subsequently converted into strong Lewis acid sites after calcination [30]. The MnCe/TNT exhibited an enriched Mn^{4+} than MnCe and MnCe/TiO_2 (Table S3), which suggested that more electrons had been transferred from Mn^{3+} to Ce^{4+} and led to an enhancement of Mn^{4+} and Ce^{3+}. The higher electron-accepting ability of Mn^{4+} also contributed to the increment of Lewis acidity [31]. The order of Lewis acidity intensity followed MnCe/TNT > MnCe/TiO_2 > MnCe, which was in line with the performance of both NH_3-SCR and toluene degradation (Fig. 1 and Table S3). This result could indicate a potential contribution of Lewis acidity in the DeNO_xTL process.

The EPR signals at g = 2.003 for all three catalysts were attributed to the unpaired electron trapped by oxygen vacancies (Vo). MnCe/TNT possessed a remarkably higher concentration of Vo than those of MnCe/TiO_2 and MnCe (Fig. 5(b)). Raman spectroscopy was used to further investigate Vo over MnCe/TNT, MnCe/TiO_2 and MnCe (Fig. S7). It was generally accepted that CeO_2 exhibited a strong Raman band at 458 cm^{-1} and a shoulder at ~600 cm^{-1}, which were denoted as the F_{2g} vibration and defect-induced modes (D band) of the CeO_2 fluorite phase, respectively [32]. The F_{2g} band of MnCe/TNT clearly shifted to 400 cm^{-1}, along with an enhancement of the D band, suggesting that Mn cations were introduced into CeO_2 and generated lattice defects [33]. The substitution of Ce^{4+} by Mn^{n+} into the CeO_2 lattice induced additional lattice perturbations and structural strain, which contributed to Vo formation [27,33]. According to the XPS results, the ratio of Mn^{4+}/Mn^{3+} and Ce^{3+}/Ce were found to both increase after the introduction of TNT on MnCe, indicating that TNT enhanced the interaction between Mn^{4+}/Mn^{3+} and Ce^{4+}/Ce^{3+} ($Ce^{4+} + Mn^{3+} \rightarrow Ce^{3+} + Mn^{4+}$), which facilitated $Ce^{4+} \rightarrow Ce^{3+} + [O]$ reaction corresponded to abundant Vo formation [13]. The area ratio of F_{2g} and D (F_{2g}/D) could reflect the Vo concentration [33], and MnCe/TNT exhibited the largest F_{2g}/D value (Table S3), which was in good accordance with EPR results. Oxygen vacancies could promote O_2 activation to form adsorbed oxygen (O_2^-, O_2^{2-}, and O^-) and facilitate lattice oxygen (O^{2-}) transport [34]. Meanwhile, the Ti 2*p* peaks of MnCe/TNT and MnCe/TiO_2 only showed Ti^{4+}

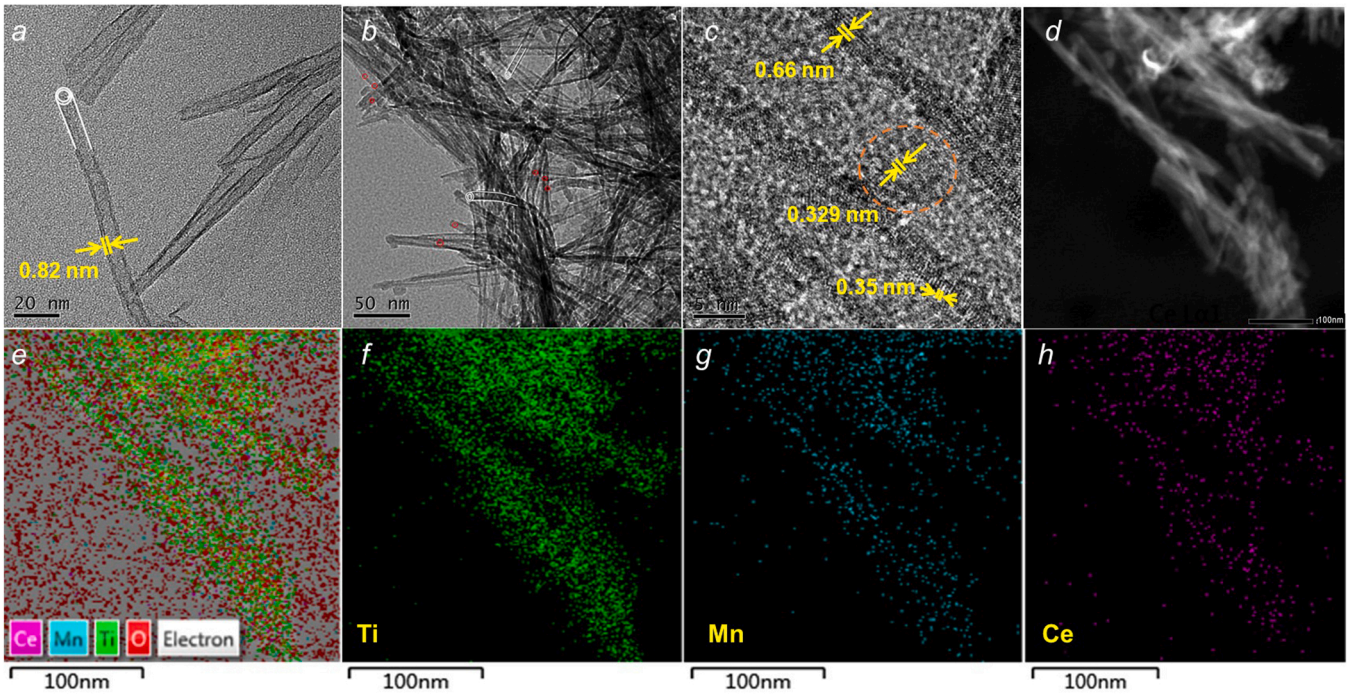

Fig. 3. (a) TEM images of TNTs, (b-d) TEM, HRTEM and HAADF-STEM images and (e-h) EDS mapping of Ti, Mn, Ce and O elements of MnCe/TNT.

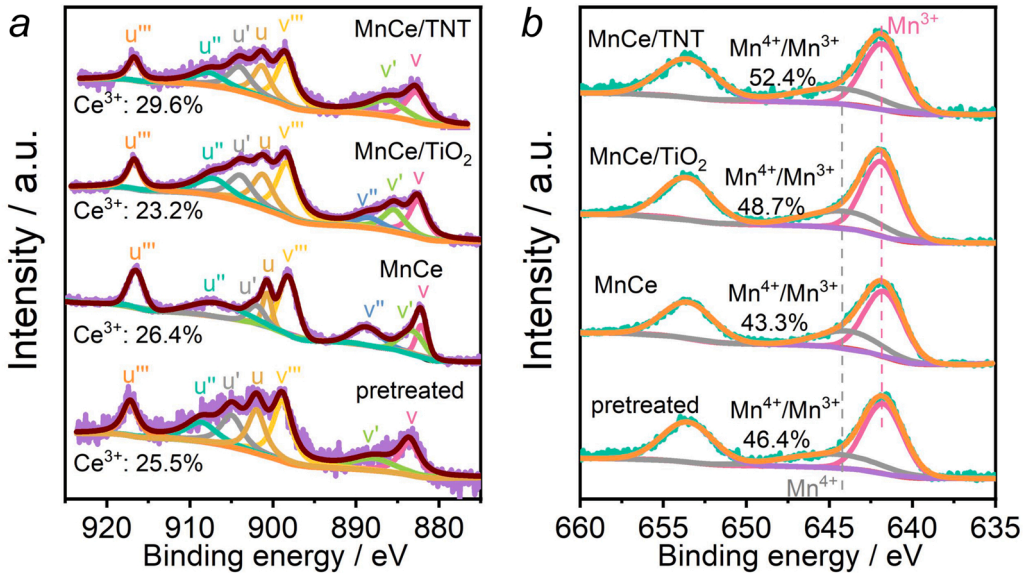

Fig. 4. XPS spectra of (a) Ce 3*d* and (b) Mn 2*p* of the MnCe, MnCe/TiO_2, MnCe/TNT, and toluene-pretreated MnCe/TNT catalysts.

peaks but no Ti^{3+} peaks, and the intensity of Ti^{4+} over MnCe/TNT was stronger than that over MnCe/TiO_2 (Fig. S8). It indicated that more Ti^{4+}–O_2^{2-}–Ce^{3+} groups existed on the MnCe/TNT catalyst surface, which was beneficial for the De*NO$_x$TL* process [35].

It was found that N_2 selectivity was sensitive to H_2 consumption amount, which reflected the reducibility of catalysts. The reducibility followed the order of MnCe > MnCe/TiO_2 > MnCe/TNT, which was well coincident with the decline rate of N_2 selectivity over MnCe, MnCe/TiO_2, and MnCe/TNT (Fig. 1(a) and Table S3). The appropriate redox ability of MnCe/TNT played an essential role in the high N_2 selectivity.

3.3. The adsorption and activation of NH_3, NO_x and toluene

As shown in the NH_3-TPD profiles, the NH_3 desorption concentration was remarkably decreased with toluene addition, indicating a competitive adsorption between NH_3 and toluene over MnCe/TNT (Fig. S10 and Table S4). This was further proven by *in situ* DRIFTs spectra, in which the intensities of coordinated NH_3 (1176 and 1193 cm^{-1}) decreased and the peak width at 1598 cm^{-1} became narrower when NH_3 and C_7H_8 co-adsorption (Fig. S11). The results of Py-IR directly demonstrated that toluene occupied the Lewis acid sites, leading to a significant decline in Lewis acid concentration and NH_3 adsorption amount (Fig. S12). However, there was an increasing number of Brønsted acid sites after toluene pretreatment (Table S4). It was reported that the dissociated free H atoms from toluene could react with available surface O and then were converted into Brønsted acids ($C_6H_5CH_3$* + O*→$C_6H_5CH_2$* + Brønsted) [36]. The changes in the acidities related to the decline of Mn^{4+} and Ce^{3+} after toluene treatment were further confirmed by XPS analysis

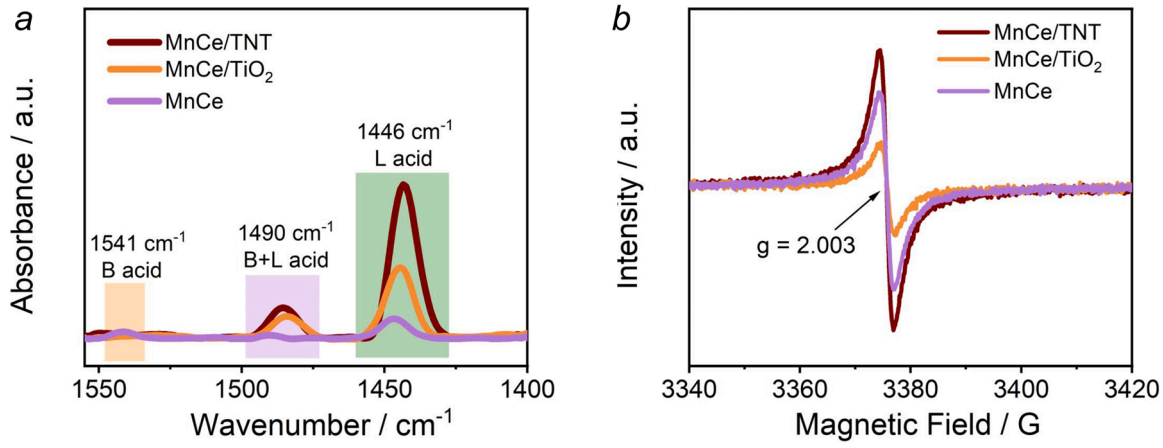

Fig. 5. (a) Pyridine-IR and (b) low-temperature (77 K) EPR spectra of MnCe/TNT, MnCe and MnCe/TiO_2.

(Table S4). The newly formed Brønsted acid sites could provide additional active sites for NH_3-SCR reaction.

Non-selective catalytic reduction reaction (NSCR) and catalytic oxidation reaction (NH_3-CO) of NH_3 are the two major pathways of N_2O formation. Toluene decreased the N_2O concentration from the NSCR process (Fig. S13(a)). Besides, NH_3-CO results illustrated that NH_3 conversion and N_2O generation were also inhibited by toluene (Fig. S13 (b)). Therefore, it was deduced that more NH_3 could be reserved for the SCR reaction rather than being oxidized into N_2O in the presence of toluene. The strong oxidative species directly influenced the activation of NH_3 [37]. Toluene decomposition would consume O_{ads}, as verified by O 1*s* XPS results (Tabel S4). Less O_{ads} and rational reducibility of MnCe/TNT would inhibit the deeper oxidation of NH_3 and further formation of NH species, leading to less N_2O generation [38].

In addition, an obvious suppression effect of toluene on NO_2 formation was found in NO catalytic oxidation (Fig. S14(a)). The formation of NO_2 was also restrained by toluene during the De*NO_xTL* process (Fig. S14(b)), and the loss of NO_2 was speculated to participate in toluene oxidation. The presence of toluene led to a decrease in NO_2/NO_x ratio (Fig. S14(c)), suggesting an adverse effect on the "fast-SCR" process. The intensities of nitrite (1254, 1476, 1314, 1495 cm^{-1}) and nitrate (1576, 1602 cm^{-1}) increased with NO + O_2 continuous addition (Fig. S15(a)). However, the peaks ascribed to bidentate nitrate (1576 cm^{-1}) and bridging nitrate (1602 cm^{-1}) disappeared when toluene was introduced (Fig. S15(b)). Since nitrate species were inactive and would suppress the catalytic oxidation activity [39], the formation of less nitrate could be helpful to toluene oxidation.

The Py-IR results demonstrated that the amount of Lewis acid sharply decreased from 0.082 to 0.058 mmol/g after toluene treatment on MnCe/TNT (Table S4), indicating that toluene was able to be adsorbed on or interact with the Lewis acid sites. *In situ* DRIFTs of toluene adsorption were carried out (Fig. S16), the bands assigned to the skeleton vibrations of the aromatic ring (1595, 1535 and 1494 cm^{-1}), the bending vibrations of a methylene group (1302 cm^{-1}), and the asymmetric methyl bending vibrations (1450 and 1416 cm^{-1}) were clearly observed (Table S5). At this time, toluene was associated with Lewis acid to form π complexes [17]. The bands at 1558, 1403, and 1323 cm^{-1} attributed to the benzaldehyde, benzoate species, and benzyl alcohol species, respectively, synchronously appeared [9,40,41]. During this step, the methyl group of these π complexes became immediately activated and underwent hydrogen abstraction, resulting in the benzyl alcohol species and benzaldehyde accumulation [42]. Importantly, the bands ascribed to the interaction of benzaldehyde with Lewis acid sites were obviously found at peaks of 1636, 1663 and 1698 cm^{-1} [43]. The interaction between carbonyl group and Lewis acid sites made the easier nucleophilic attack of surface adsorbed oxygen on the carbon atom of benzaldehyde and facilitated the formation of benzoate species [17,42]. Therefore, *in situ* DRIFTs analysis well demonstrated that the plentiful Lewis acid sites of MnCe/TNT could efficiently capture and activate toluene molecules, resulting in rapid dehydrogenation to generate benzoate species with the assistance of oxygen vacancies (O_{ads}).

3.4. Mechanism study

3.4.1. NH_3-SCR

A series of time-resolved *in situ* DRIFTs spectra were conducted to evaluate the transient reaction between adsorbed NH_3 (+C_7H_8) with gaseous NO + O_2 over MnCe/TNT. The coordinated NH_3 linked to Lewis acid sites (1176, 1193, 1598 and 1641 cm^{-1}) was quickly consumed by NO + O_2 within 2 min (Fig. 6(a, b)). The coordinated NH_3 was active to directly react with gaseous NO through the Eley-Rideal (E-R) mechanism, and then decomposed into N_2 and N_2O. After NO + O_2 were introduced into NH_3 and toluene pretreated catalyst, the bands at 1598 and 1641 cm^{-1} were sluggishly decreased (Fig. 6(d, e)), indicating that toluene could inhibit the reactivity of adsorbed NH_3 through the E-R mechanism.

The tail-end concentration of NO, NO_2 and N_2O of the *in situ* DRIFTs were monitored in real-time (called *operando*-DRIFTs). NO + O_2 reacted quickly with NH_3, resulting in a maximum N_2O concentration of ~14.0 ppm at ~1 min. The N_2O formation was significantly suppressed by the presence of toluene and the maximum N_2O concentration was decreased to ~7.0 ppm (Fig. 6(c, f)). The NSCR reaction via the E-R mechanism was restrained by toluene, leading to the reduction of N_2O generation. The *operando*-DRIFTs further confirmed that NO_2 formation and NO adsorption would be restricted by toluene. Besides, the intensity of N_2 noticeably fell down when passing NO_x over the NH_3 + C_7H_8 pre-exposed surface (Fig. S17). Toluene would weaken the SCR activity through the E-R mechanism, thus reducing N_2 formation.

The dynamic change of *in situ* DRIFTs in a flow of NH_3 over the NO + O_2 pre-adsorbed catalyst was recorded (Fig. S18(a)). New peaks assigned to the coordinated NH_3 (1208 cm^{-1}) and NH_3 oxidation species (1555 cm^{-1}) appeared after feeding NH_3 [44,45]. The bands corresponding to nitrite species were feebly decreased when being exposed to NH_3, while the intensities of cis-$N_2O_2^{2-}$ (1382 cm^{-1}), trans-$N_2O_2^{2-}$ (1405 cm^{-1}) and nitrate species (1576 and 1602 cm^{-1}) were slightly increased at the same time. The consumption of a small amount of nitrite suggested that Langmuir-Hinshelwood (L-H) mechanism could help the reduction of NO to form N_2, but the contribution was much less than that of the E-R mechanism. Likewise, there was no obvious decrease in nitrite when feeding NH_3 over NO + O_2 + C_7H_8 pre-adsorbed catalyst (Fig. S18 (b)). It was also difficult to identify the effect of toluene on N_2 formation through L-H mechanism according to *operando*-DRIFTs (Fig. S18(c)), so a further kinetic analysis was required. However, *operando*-DRIFTs clearly demonstrated that only a small amount of N_2O was generated

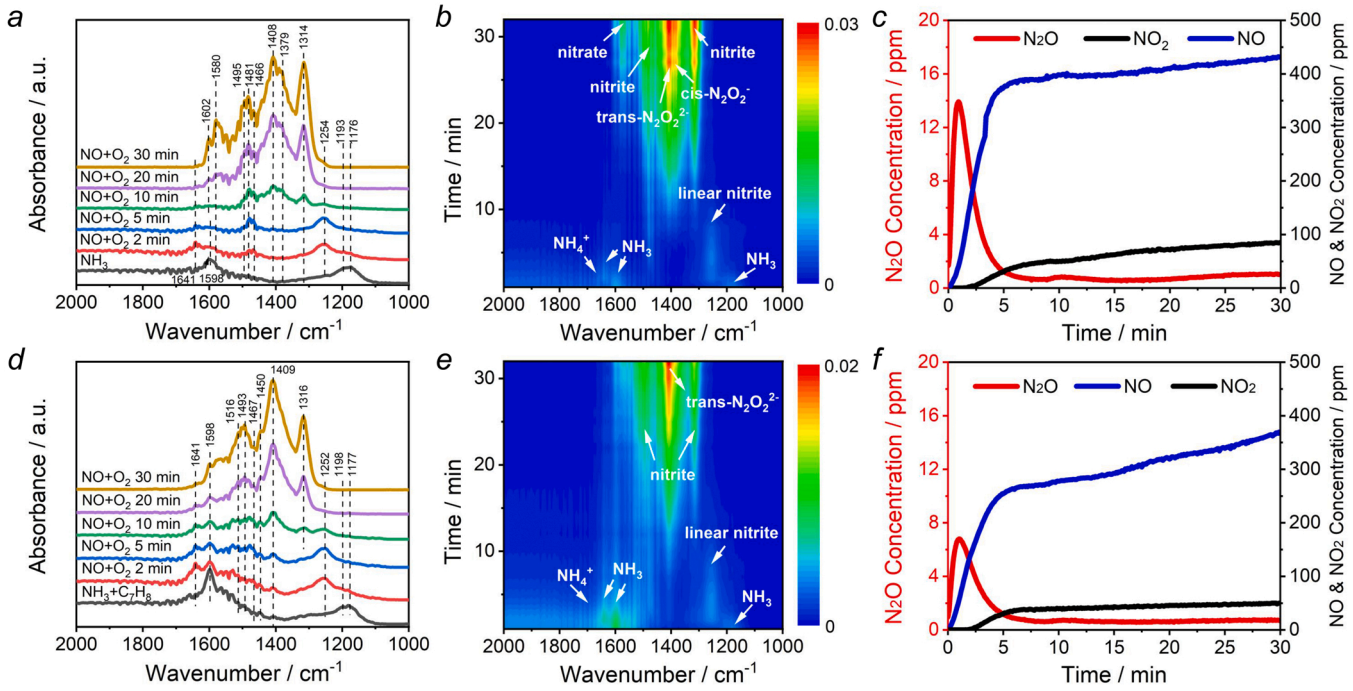

Fig. 6. (a-b) *in situ* DRIFTs and (c) NO_x and N_2O concentrations when passing $NO+O_2$ over NH_3 pre-adsorbed catalyst at 200 °C, (d-e) *in situ* DRIFTs and (f) NO_x and N_2O concentrations when passing $NO+O_2$ over NH_3 $+C_7H_8$ pre-adsorbed catalyst at 200 °C.

during the NSCR process through the L-H mechanism. The maximum N_2O concentration formed from E-R mechanism was ~3.5-times higher than those through the L-H mechanism (Fig. 6(c) and Fig. S18(d)). When exposed to toluene, the maximum N_2O concentration through the L-H mechanism dropped from ~3.2 ppm to ~1.6 ppm. These results indicated that the NSCR process through L-H mechanism would be inhibited by toluene, leading to the reduction of N_2O formation.

The formation of N_2 was linear with gaseous NO concentration, which suggested the reaction order was 1 (Fig. 7(a, b)). This result was in line with NH_3-SCR steady-state kinetics [46,47] (see Eq. 1), which can identify the contribution of the E-R and L-H mechanisms in the formation of N_2.

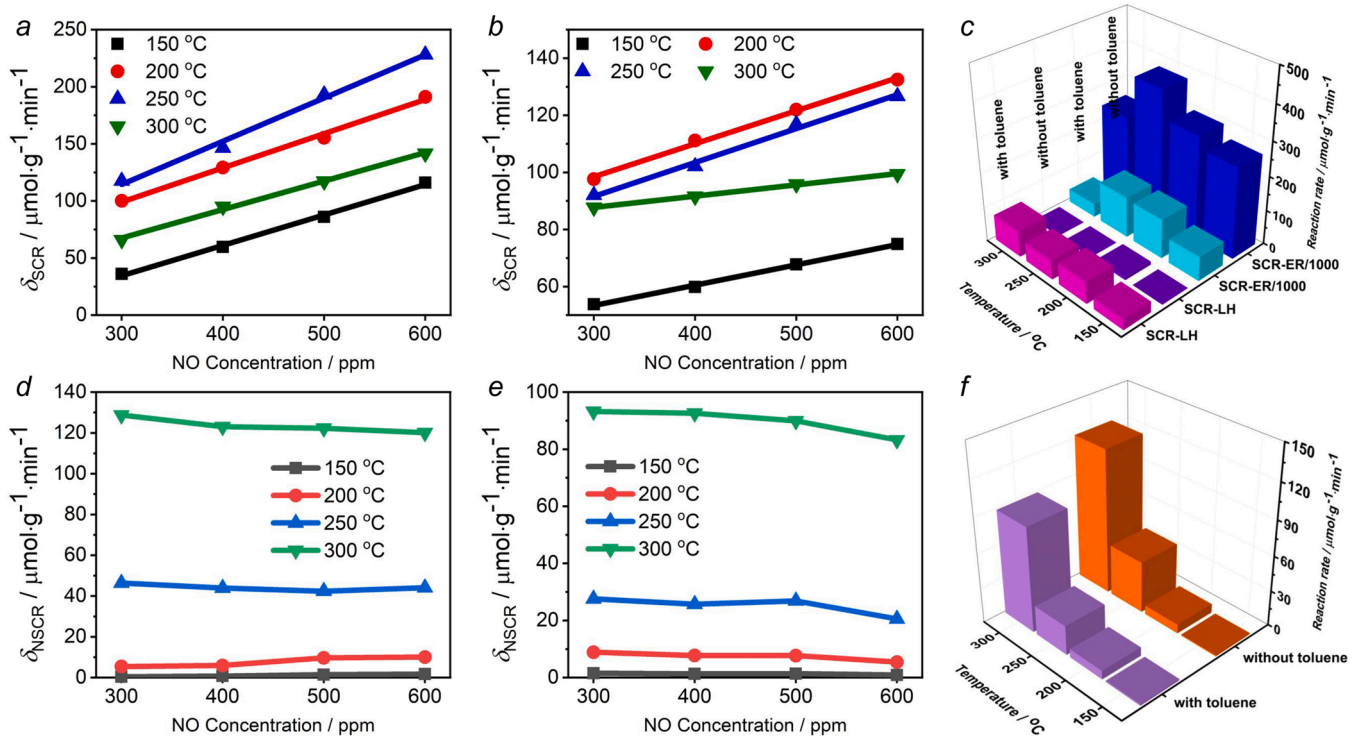

Fig. 7. N_2 formation rate of the SCR reaction path (a) without, (b) with toluene and (c) quantitative analysis of the SCR reaction. N_2O formation rate of the NSCR reaction path (d) without, (e) with toluene and (f) quantitative analysis of the NSCR reaction. Reaction conditions: $[NH_3]$ = 500 ppm, [NO] = 300–600 ppm, [Toluene] = 50 ppm (when used), $[O_2]$ = 10 vol.%, catalyst mass = 5–10 mg, total flow rate = 400 mL/min and GHSV = 2400,000–4800,000 mL/(g·h).

$$\frac{d[N_2]}{dt} = \delta_{SCR} = k_{SCR-LH} + k_{SCR-ER}[NO_{(g)}] \quad (1)$$

The intercept ($k_{SCR\text{-}LH}$) of Eq. (1) was greater than 1, indicating that L-H mechanism influenced the deNO$_x$ process and could not be ignored (Table S6). However, the rate constants through the E-R mechanism ($k_{SCR\text{-}ER}$) accounted for up to ~99% of the SCR reaction, indicating that E-R mechanism controlled the NO reduction, and served as the rate-determining step of N_2 formation. L-H mechanism was not the contributor to NH_3-SCR over MnCe/TNT. After the addition of toluene, $k_{SCR\text{-}ER}$ was significantly decreased. This demonstrated that toluene suppressed N_2 generation through the E-R mechanism. However, the presence of toluene led to the increasing $k_{SCR\text{-}LH}$, which intuitively demonstrated that NH_3-SCR activity through L-H mechanism was promoted by toluene (Fig. 7(c) and Table S6). As NH_3-SCR reaction was less controlled by L-H mechanism, toluene would just result in a little N_2 formation.

As shown in Fig. 7(d, e), the rate of NSCR reaction was far different from that of SCR. The reaction order of N_2O formation with respect to gaseous NO concentration was approximately zero, which met the description of Eq. (2) [48]. The rate constant of the NSCR reaction (k_{NSCR}) was notably decreased with the addition of toluene, especially above 150 °C (Fig. 7(f) and Table S6). The kinetic analysis demonstrated that the N_2O formation over MnCe/TNT through NSCR reaction was suppressed by toluene.

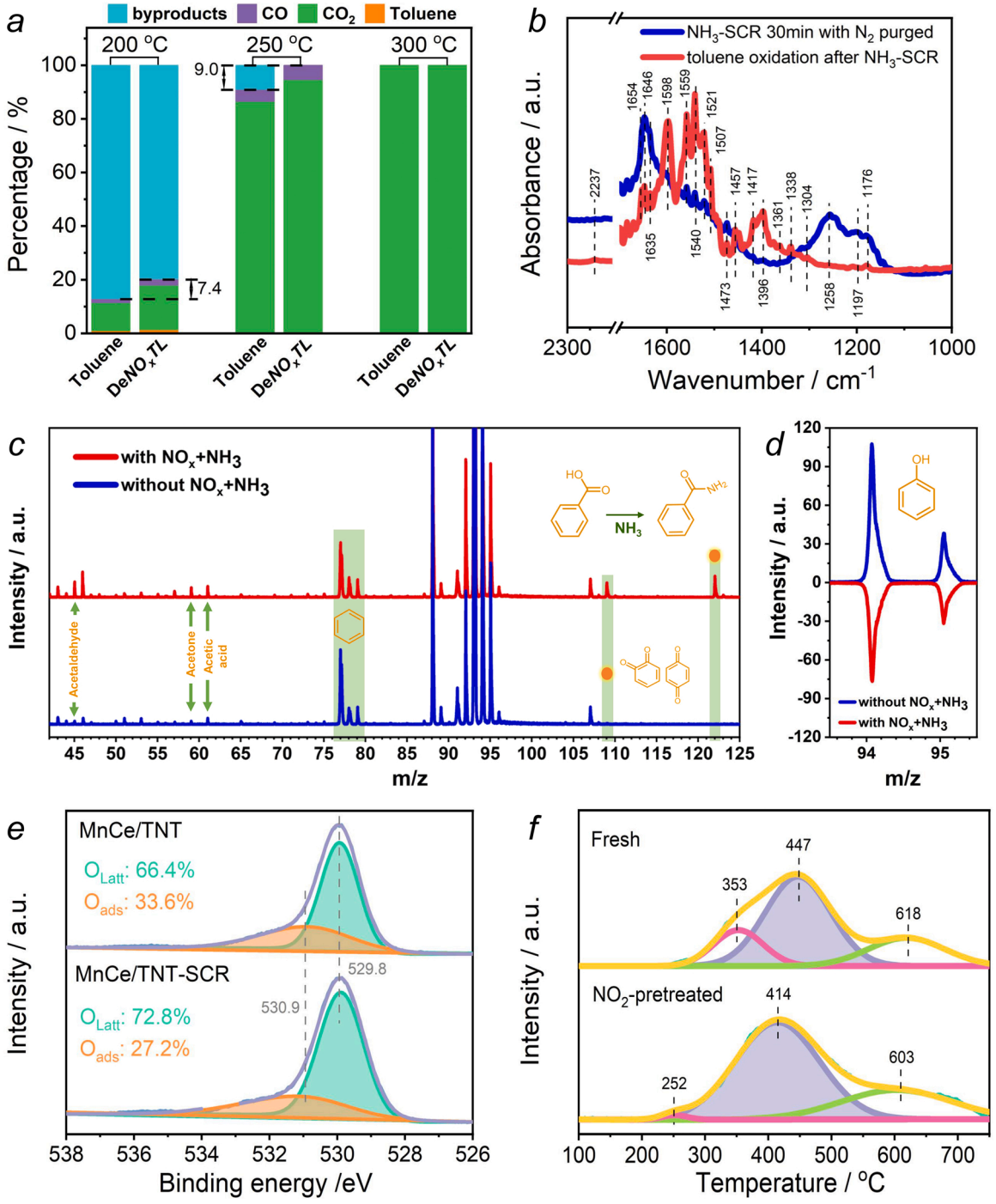

Fig. 8. (a) Carbon balance analysis in the outlet gas, (b) *in situ* DRIFTs spectra recorded at 200 °C of toluene oxidation after NH_3-SCR reaction, (c-d) PTR-ToF-MS spectra of gaseous by-products in the outlet gas, (e) O 1 *s* XPS spectra, (f) O_2-TPD profiles of fresh and NO_2-pretreated catalysts.

$$\frac{d[N_2O]}{dt} = k_{NSCR-LH} + k_{NSCR-ER} = k_{NSCR} \quad (2)$$

Since the macroscopical N_2 selectivity was not affected by the addition of toluene (Fig. 2), it meant that the decrement of N_2O should be more than the amount of N_2 that was restrained by toluene from SCR through E-R mechanism. Therefore, the inhibitory effect of toluene on the NSCR and NH_3-CO reaction was crucial for the decrease of N_2O formation, which largely guaranteed the high and stable N_2 selectivity during the De*NO$_x$TL* process over MnCe/TNT.

3.4.2. Toluene oxidation

With the increase of temperature, the interaction of carbonyl group with Lewis acid became dramatic along with the intensities of 1636, 1663 and 1698 cm^{-1} significantly increased during toluene oxidation. Lewis acid facilitated the nucleophilic attack of adsorbed oxygen (O_{ads}) on benzaldehyde, resulting in a large formation of benzoate species (1396, 1521 and 1541 cm^{-1}) (Fig. S19). It has been proved that ring-opening of the adsorbed benzoate species was caused by the attack of basic nucleophilic lattice oxygen (O^{2-}) and Lewis acid [49,50]. The bands attributed to the maleic anhydride (1306 cm^{-1}) [9], oxalic acid (1417 cm^{-1}) [51], surface carbonate species (1360 cm^{-1}) [42] and CO_2 (2359 and 2340 cm^{-1}) [52] gradually appeared, which implied the attack by lattice oxygen and Lewis acid upon the carbon structures as well as the opening of aromatic ring and the formation of CO_2. Besides, the prolonged residence time due to diffusion limitations inside the TNT channels facilitated the oxidation of aromatic ring to form primary chain species and carbon oxides [53].

When SCR reactants were added into the gaseous stream, more CO_2 was generated while the gaseous byproducts were remarkably decreased by 9.0% at 250 °C (Fig. 8(a)). Toluene was more prone to be deeply oxidized into primary chain species and CO_2 with the help of NH_3 and NO_x. When MnCe/TNT catalyst was exposed to NO +NH_3 +O_2 at 200 °C for 30 min (Fig. 8(b)), the bands related to nitrite (1473 and 1258 cm^{-1}), nitrate (1521, 1541 and 1559 cm^{-1}) and the adsorbed NO_2 (1635 cm^{-1}) appeared [54–56]. NH_4^+ species adsorbed on the Brønsted acid sites (1507 cm^{-1}) [57] and NH_3 species coordinated to the Lewis acid sites (1176, 1197 and 1646 cm^{-1}) [47,58] were also observed. After switching to C_7H_8 + O_2 gas, the bands attributed to Lewis acid and nitrite disappeared within 10 min, meanwhile, the band corresponding to the adsorbed NO_2 significantly diminished. Subsequently, new bands assigned to benzyl alcohol (1338 cm^{-1}), benzoate species (1396, 1521 and 1541 cm^{-1}), benzaldehyde (1559 cm^{-1}), maleic anhydride (1306 cm^{-1}), oxalic acid (1417 cm^{-1}), surface carbonate species (1360 cm^{-1}), and nitrile species (δ(C≡N), 2237 cm^{-1}) [37] were found. The main gaseous by-products during the De*NO$_x$TL* process, including acetone, acetic acid, benzaldehyde, benzoquinone, and benzoic acid, etc., were identified by PTR-ToF-MS (Fig. 8(c, d) and Table S7). Benzamide ($PhCONH_2$) as a product from the reaction between NH_3 and benzaldehyde or benzoic acid was detected concurrently. Compared with mixture gas condition (NH_3 +NO+O_2 +C_7H_8), the amount of formic acid, acetone, acetic acid and propanoic acid dramatically dropped, while more benzene and phenol accumulation were identified during toluene oxidation without NH_3 + NO_x. It was confirmed by XPS that the SCR reactants were able to enhance the lattice oxygen over the MnCe/TNT (Fig. 8(e)). The ratio of lattice oxygen of the SCR-used catalyst increased to 72.8% compared to that of fresh catalyst (66.4%).

Adsorbed O_2 could be generally activated by Ce^{3+} located outside the oxygen vacancies [35], following the procedure of O_2(ads) → O_2^-(ads) → O_2^{2-}(ads) → O^-(ads) → O^{2-} (lattice), during which Ce^{3+} lost electrons and changed into Ce^{4+}. The Ce^{4+} provided lattice oxygen to oxidize toluene as in the step of the MvK mechanism, with Ce^{4+} changed into Ce^{3+}. In the following step, these Ce^{3+} species would be again re-oxidized by adsorbed O_2. Moreover, the lattice oxygen of Mn^{4+} could be activated by Ce^{3+} cations through the Zener exchange, resulting in more content and mobility of lattice oxygen for toluene oxidation [28].

The *in-situ* generated NO_2 during the De*NO$_x$TL* process was a stronger oxidant than O_2 and could give one of its O into the shorter reaction chain of NO_2(ads) → O^-(ads) → O^{2-} (lattice) [36]. O_2-TPD was employed to study surface oxygen species. Adsorbed oxygen (O_{ads}) species first desorb in the ranges of 100 – 400 °C, followed by the desorption of surface lattice oxygen (O_{latt}) at 400 – 550 °C, and finally bulk O_{latt} at > 550 °C [19]. As shown in Fig. 8(f), the surface O_{latt} desorption temperature of NO_2-pretreated catalyst (414 °C) was lower than that of fresh catalyst (447 °C), and the proportion of O^{2-} increased from 59.9% to 71.5%, indicating that NO_2 could speed up the Mn^{4+} + Ce^{3+} ↔ Mn^{3+} + Ce^{4+} circulation, and improve the content and mobility of O^{2-}.

The analysis of the residual intermediates on the catalyst surface was carried out (Fig. S22 and Table S8). Acetonitrile, benzene, toluene, benzaldehyde and benzonitrile were detected on the surface of catalyst used in toluene oxidation with NH_3 + NO (assigned as "simultaneous-used" catalyst). Toluene oxidation byproducts (e.g., carboxylic and aldehyde compounds) easily reacted with NH_3 through nucleophilic addition and dehydration to produce nitrile species [59]. However, the TG analysis showed that there was only ~1.5% of massive weight loss of the catalyst used in the De*NO$_x$TL* process compared with fresh catalyst (Fig. S23). It reflected that the De*NO$_x$TL* activity was less influenced by the residual intermediates.

Combined with the results of *in situ* DRIFTs, PTR-ToF-MS and TG-GC-MS, it revealed that toluene molecule adsorption and activation occurred rapidly at the Lewis acid sites, followed by the attack of the basic nucleophilic lattice oxygen (O^{2-}). The aromatic ring of toluene was effectively cracked in the effect of NO_2 and Lewis acid without benzene and phenol species aggregation, which significantly facilitated the removal and mineralization of toluene. The cooperation of Lewis acid site and oxygen vacancies played an essential role in lowering toluene conversion temperature and facilitating toluene catalytic oxidation. The aldehyde and carboxylic compounds would react with the coordinated NH_3 to yield the corresponding nitrile coke and gaseous amide species. In line with this, NO_x was adsorbed on the catalyst surface to produce the adsorbed NO_2^-, which combined with the amide species to form N_2 during the De*NO$_x$TL* process. The nitrogen (N) element from the NH_3 and NO_x was migrated and transformed through the above routes.

In summary, the possible reaction pathway of the De*NO$_x$TL* process over MnCe/TNT catalyst was displayed in Fig. 9. Lewis acid sites and oxygen vacancies were concurrently generated when Mn^{3+} + Ce^{4+} shifted to Mn^{4+} + Ce^{3+}. The TiO_2 nanotubes improved the electron interaction between Mn^{4+}/Mn^{3+} and Ce^{4+}/Ce^{3+}, further facilitating the oxygen activation capacity and Lewis acidity. Under a rational reducibility of MnCe/TNT, Lewis acid sites and oxygen vacancies synergistically promoted NH_3-SCR and toluene oxidation. Nitric oxide predominantly reacted with NH_3 coordinated to Lewis acid sites, followed by the E-R mechanism to form N_2 (blue route). Toluene decomposition consumed O_{ads} (O^-) and prevented NH_3 from participating in the NSCR and the NH_3-CO reactions, which remarkably inhibited the N_2O formation and ensured a high N_2 selectivity over 90%. Along with NH_3-SCR, the newly generated strong oxidant NO_2 took part in toluene oxidation (green route) via the MvK mechanism, thus accelerating Mn^{4+} + Ce^{3+} ↔ Mn^{3+} + Ce^{4+} circulation and increasing the mobility of O_{latt} (O^{2-}). Toluene adsorption and dissociation occurred rapidly at the Lewis acid sites with O_{ads} (O^-), and its ring-opening benefited from the assistance of the O_{latt} (O^{2-}) and Lewis acid. The nitrogen element from the NH_3 was migrated and transformed into nitrile coke and gaseous amide species, while the adsorbed NO_2^- combined with the amide species to form N_2.

4. Conclusion

In this study, the as-tailed MnCe/TNT catalyst exhibited excellent low-temperature NO_x and toluene co-removal performance with good

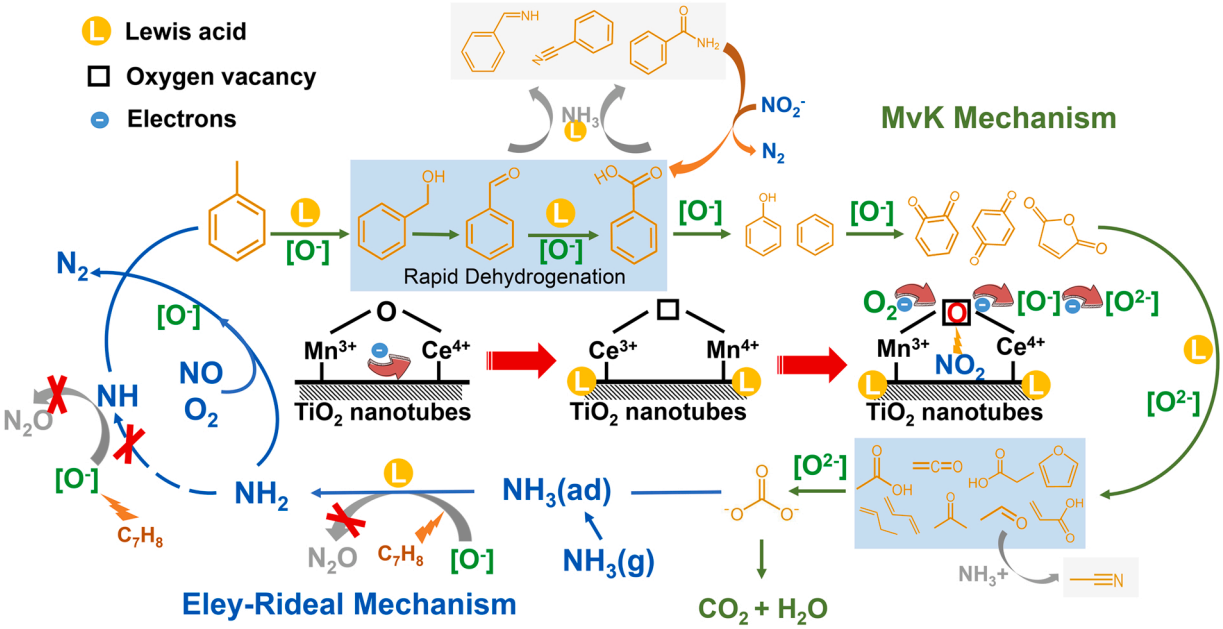

Fig. 9. The possible reaction pathway of the DeNO_xTL process over MnCe/TNT.

H_2O durability. The synergistic effect of Lewis acid and oxygen vacancies was originally demonstrated for boosting the simultaneous removal of NO_x and toluene. The improvement of Lewis acidity could be an effective approach to lower the toluene conversion temperature without enhancing the redox ability and stabilize high N_2 selectivity. Our research sheds substantial light on the rational design of environmental catalysts for simultaneous catalytic removal of NO_x and VOCs from industrial flue gas.

CRediT authorship contribution statement

Lyumeng Ye: Conceptualization, Methodology, Validation, Data curation, Formal analysis, Investigation, Writing – original draft, Writing – review & editing. **Peng Lu:** Resources, Data curation, Writing – review & editing, Funding acquisition. **Xianhui Yan:** Validation, Formal analysis, Investigation. **Haibao Huang:** Methodology, Resources, Writing – review & editing, Supervision, Project administration, Funding acquisition.

Declaration of Competing Interest

The authors declare that they have no known competing financial interests or personal relationships that could have appeared to influence the work reported in this paper.

Data Availability

The authors do not have permission to share data.

Acknowledgments

This work was financially supported by the National Key Research and Development Plan of China (2022YFC3701700), the National Natural Science Foundation of China (22076224, 22276223), Guangdong Basic and Applied Basic Research Foundation (2022A1515110085), Guangdong Province Engineering Laboratory for Air Pollution (2019323609-01), the Project of Science and Technology Program of Guangzhou, China (202102020135), and the Program for Guangdong Introducing Innovative and Entrepreneurial Teams (2017ZT07C069).

Appendix A. Supporting information

Supplementary data associated with this article can be found in the online version at doi:10.1016/j.apcatb.2023.122696.

References

[1] D. Wang, Q. Chen, X. Zhang, C. Gao, B. Wang, X. Huang, Y. Peng, J. Li, C. Lu, J. Crittenden, Multipollutant control (MPC) of flue gas from stationary sources using SCR technology: A critical review, Environ. Sci. Technol. 55 (2021) 2743–2766.
[2] M. Gallastegi-Villa, A. Aranzabal, J.A. González-Marcos, J.R. González-Velasco, Tailoring dual redox-acid functionalities in VO_x/TiO_2/ZSM5 catalyst for simultaneous abatement of PCDDFs and NO_x from municipal solid waste incineration, Appl. Catal., B 205 (2017) 310–318.
[3] L. Gan, K. Li, S. Xiong, Y. Zhang, J. Chen, Y. Peng, J. Li, MnO_x-CeO_2 catalysts for effective NO_x reduction in the presence of chlorobenzene, Catal. Commun. 117 (2018) 1–4.
[4] C. Zhang, J. Zhang, Y. Shen, J. He, W. Qu, J. Deng, L. Han, A. Chen, D. Zhang, Synergistic catalytic elimination of NO_x and chlorinated organics: cooperation of acid sites, Environ. Sci. Technol. 56 (2022) 3719–3728.
[5] Y. Ji, J. Zhao, H. Terazono, K. Misawa, N.P. Levitt, Y. Li, Y. Lin, J. Peng, Y. Wang, L. Duan, Reassessing the atmospheric oxidation mechanism of toluene, Proc. Natl. Acad. Sci. 114 (2017) 8169–8174.
[6] X.M. Liang, X.B. Sun, J.T. Xu, D.Q. Ye, Improved emissions inventory and VOCs speciation for industrial OFP estimation in China, Sci. Total Environ. 745 (2020), 140838.
[7] C. Stockwell, P. Veres, J. Williams, R. Yokelson, Characterization of biomass burning emissions from cooking fires, peat, crop residue, and other fuels with high-resolution proton-transfer-reaction time-of-flight mass spectrometry, Atmos. Chem. Phys. 15 (2015) 845–865.
[8] C. Braguglia, G. Bagnuolo, A. Gianico, G. Mininni, C. Pastore, G. Mascolo, Preliminary results of lab-scale investigations of products of incomplete combustion during incineration of primary and mixed digested sludge, Environ. Sci. Pollut. R. 23 (2016) 4585–4593.
[9] X. Yang, X. Yu, M. Jing, W. Song, J. Liu, M. Ge, Defective $Mn_xZr_{1-x}O_2$ solid solution for the catalytic oxidation of toluene: insights into the oxygen vacancy contribution, ACS Appl. Mater. Interfaces 11 (2018) 730–739.
[10] Y. Chen, Y. Liao, L. Chen, Z. Chen, X. Ma, Performance of transition metal (Cu, Fe and Co) modified SCR catalysts for simultaneous removal of NO and volatile organic compounds (VOCs) from coal-fired power plant flue gas, Fuel 289 (2021), 119849.
[11] L. Chen, Y. Liao, Y. Chen, J. Wu, X. Ma, Performance of Ce-modified V-W-Ti type catalyst on simultaneous control of NO and typical VOCS, Fuel Process. Technol. 207 (2020), 106483.
[12] L. Chen, Y. Liao, S. Xin, X. Song, G. Liu, X. Ma, Simultaneous removal of NO and volatile organic compounds (VOCs) by Ce/Mo doping-modified selective catalytic reduction (SCR) catalysts in denitrification zone of coal-fired flue gas, Fuel 262 (2020), 116485.

[13] L. Zhao, Y. Huang, J. Zhang, L. Jiang, Y. Wang, Al_2O_3-modified CuO-CeO_2 catalyst for simultaneous removal of NO and toluene at wide temperature range, Chem. Eng. J. 397 (2020), 125419.

[14] Z. Li, Y. Gao, Q. Wang, The influencing mechanism of NH_3 and NO_x addition on the catalytic oxidation of toluene over $Mn_2Cu_1Al_1O_x$ catalyst, J. Clean. Prod. 348 (2022), 131152.

[15] L. Ye, P. Lu, X. Chen, P. Fang, Y. Peng, J. Li, H. Huang, The deactivation mechanism of toluene on MnO_x-CeO_2 SCR catalyst, Appl. Catal., B 277 (2020), 119257.

[16] A. Marberger, D. Ferri, M. Elsener, O. Kröcher, The significance of Lewis acid sites for the selective catalytic reduction of nitric oxide on vanadium-based catalysts, Angew. Chem. Int. Ed. 55 (2016) 11989–11994.

[17] A. Corma, H. García, Lewis acids as catalysts in oxidation reactions: from homogeneous to heterogeneous systems, Chem. Rev. 102 (2002) 3837–3892.

[18] W. Yuan, S. Zhang, Y. Wu, X. Huang, F. Tian, S. Liu, C. Li, Enhancing the room-temperature catalytic degradation of formaldehyde through constructing surface lewis pairs on carbon-based catalyst, Appl. Catal., B 272 (2020), 118992.

[19] J. Yang, S. Hu, L. Shi, S. Hoang, W. Yang, Y. Fang, Z. Liang, C. Pan, Y. Zhu, L. Li, J. Wu, J. Hu, Y. Guo, Oxygen vacancies and Lewis acid sites synergistically promoted catalytic methane combustion over perovskite oxides, Environ. Sci. Technol. 55 (2021) 9243–9254.

[20] P. Wang, H. Wang, X. Chen, Y. Liu, X. Weng, Z. Wu, Novel SCR catalyst with superior alkaline resistance performance: enhanced self-protection originated from modifying protonated titanate nanotubes, J. Mater. Chem. A 3 (2015) 680–690.

[21] X. Chen, P. Wang, P. Fang, T. Ren, Y. Liu, C. Cen, H. Wang, Z. Wu, Tuning the property of Mn-Ce composite oxides by titanate nanotubes to improve the activity, selectivity and SO_2/H_2O tolerance in middle temperature NH_3-SCR reaction, Fuel Process. Technol. 167 (2017) 221–228.

[22] C. He, J. Cheng, X. Zhang, M. Douthwaite, S. Pattisson, Z. Hao, Recent advances in the catalytic oxidation of volatile organic compounds: a review based on pollutant sorts and sources, Chem. Rev. 119 (2019) 4471–4568.

[23] V.F. da Silva Filho, L. Batistella, J.L.F. Alves, J.C.G. da Silva, C.A. Althoff, Rd.F.P. M. Moreira, H.J. José, Evaluation of gaseous emissions from thermal conversion of a mixture of solid municipal waste and wood chips in a pilot-scale heat generator, Renew. Energy 141 (2019) 402–410.

[24] L. Gan, Y. Wang, J. Chen, T. Yan, J. Li, J. Crittenden, Y. Peng, The synergistic mechanism of NO_x and chlorobenzene degradation in municipal solid waste incinerators, Catal. Sci. Technol. 9 (2019) 4286–4292.

[25] Y. Zhou, X. Xing, J. Lang, D. Chen, S. Cheng, L. Wei, X. Wei, C. Liu, A comprehensive biomass burning emission inventory with high spatial and temporal resolution in China, Atmos. Chem. Phys. 17 (2017) 2839–2864.

[26] J. Chen, X. Chen, X. Chen, W. Xu, Z. Xu, H. Jia, J. Chen, Homogeneous introduction of CeO_y into MnO_x-based catalyst for oxidation of aromatic VOCs, Appl. Catal., B 224 (2018) 825–835.

[27] L. Ye, P. Lu, D. Chen, D. Chen, H. Wu, W. Dai, Y. Gan, J. Xiao, Z. Xie, Z. Li, H. Huang, Activity enhancement of acetate precursor prepared on MnO_x-CeO_2 catalyst for low-temperature NH_3-SCR: effect of gaseous acetone addition, Chin. Chem. Lett. 32 (2021) 2509–2512.

[28] J. Chen, X. Chen, D. Yan, M. Jiang, W. Xu, H. Yu, H. Jia, A facile strategy of enhancing interaction between cerium and manganese oxides for catalytic removal of gaseous organic contaminants, Appl. Catal., B 250 (2019) 396–407.

[29] W. Hong, Y. Liu, T. Zhu, H. Wang, Y. Sun, F. Shen, X. Li, Promoting the catalytic ozonation of toluene by introducing SO_4^{2-} into the α-MnO_2/ZSM-5 catalyst to tune both oxygen vacancies and acid sites, Environ. Sci. Technol. 56 (2022) 15695–15704.

[30] P. Sun, S. Zhai, J. Chen, J. Yuan, Z. Wu, X. Weng, Development of a multi-active center catalyst in mediating the catalytic destruction of chloroaromatic pollutants: a combined experimental and theoretical study, Appl. Catal., B 272 (2020), 119015.

[31] X. Weng, P. Sun, Y. Long, Q. Meng, Z. Wu, Catalytic oxidation of chlorobenzene over $Mn_xCe_{1-x}O_2$/HZSM-5 catalysts: a study with practical implications, Environ. Sci. Technol. 51 (2017) 8057–8066.

[32] Z. Wu, M. Li, J. Howe, H.M. Meyer, S.H. Overbury, Probing defect sites on CeO_2 nanocrystals with well-defined surface planes by raman spectroscopy and O_2 adsorption, Langmuir 26 (2010) 16595–16606.

[33] X. Yao, K. Ma, W. Zou, S. He, J. An, F. Yang, D. Lin, Influence of preparation methods on the physicochemical properties and catalytic performance of MnO_x-CeO_2 catalysts for NH_3-SCR at low temperature, Chin. J. Catal. 38 (2017) 146–159.

[34] Y. Zheng, K. Fu, Z. Yu, Y. Su, R. Han, Q. Liu, Oxygen vacancies in a catalyst for VOCs oxidation: synthesis, characterization, and catalytic effects, J. Mater. Chem. A 10 (2022) 14171–14186.

[35] H. Liu, J. Chen, Y. Wang, R. Yin, W. Yang, G. Wang, W. Si, Y. Peng, J. Li, Interaction mechanism for simultaneous elimination of nitrogen oxides and toluene over the bifunctional CeO_2–TiO_2 mixed oxide catalyst, Environ. Sci. Technol. 56 (2022) 4467–4476.

[36] P. Lu, L. Ye, X. Yan, X. Chen, P. Fang, D. Chen, D. Chen, C. Cen, Insight into the promotional effect of NO_2 on toluene oxidation over MnCe/HZSM-5 catalyst, Appl. Surf. Sci. 600 (2022), 154161.

[37] P. Lu, L. Ye, X. Yan, P. Fang, X. Chen, D. Chen, C. Cen, Impact of toluene poisoning on MnCe/HZSM-5 SCR catalyst, Chem. Eng. J. 414 (2021), 128838.

[38] P. Lu, L. Ye, X. Yan, X. Chen, P. Fang, D. Chen, D. Chen, C. Cen, N_2O inhibition by toluene over Mn-Fe spinel SCR catalyst, J. Hazard. Mater. 414 (2021), 125468.

[39] L. Ye, P. Lu, Y. Peng, J. Li, H. Huang, Impact of NO_x and NH_3 addition on toluene oxidation over MnO_x-CeO_2 catalyst, J. Hazard. Mater. 416 (2021), 125939.

[40] S. Mo, Q. Zhang, J. Li, Y. Sun, Q. Ren, S. Zou, Q. Zhang, J. Lu, M. Fu, D. Mo, J. Wu, H. Huang, D. Ye, Highly efficient mesoporous MnO_2 catalysts for the total toluene oxidation: Oxygen-Vacancy defect engineering and involved intermediates using in situ DRIFTS, Appl. Catal., B 264 (2020), 118464.

[41] Y. Wang, J. Wu, G. Wang, D. Yang, T. Ishihara, L. Guo, Oxygen vacancy engineering in Fe doped akhtenskite-type MnO_2 for low-temperature toluene oxidation, Appl. Catal., B 285 (2021), 119873.

[42] W. Yang, Za Su, Z. Xu, W. Yang, Y. Peng, J. Li, Comparative study of α-, β-, γ-and δ-MnO_2 on toluene oxidation: Oxygen vacancies and reaction intermediates, Appl. Catal., B 260 (2020), 118150.

[43] G. Centi, S. Perathoner, S. Tonini, In situ DRIFT study of the reactivity and reaction mechanism of catalysts based on iron–molybdenum oxides encapsulated in Boralite for the selective oxidation of alkylaromatics, Catal. Today 61 (2000) 211–221.

[44] F. Liu, H. He, C. Zhang, W. Shan, X. Shi, Mechanism of the selective catalytic reduction of NO_x with NH_3 over environmental-friendly iron titanate catalyst, Catal. Today 175 (2011) 18–25.

[45] G. Qi, R.T. Yang, Characterization and FTIR Studies of MnO_x-CeO_2 Catalyst for Low-Temperature Selective Catalytic Reduction of NO with NH_3, J. Phys. Chem. B 108 (2004) 15738–15747.

[46] S. Xiong, Y. Liao, X. Xiao, H. Dang, S. Yang, Novel Effect of H_2O on the Low Temperature Selective Catalytic Reduction of NO with NH_3 over MnO_x-CeO_2: Mechanism and Kinetic Study, J. Phys. Chem. C. 119 (2015) 4180–4187.

[47] D. Wang, Y. Peng, S. Xiong, B. Li, L. Gan, C. Lu, J. Chen, Y. Ma, J. Li, De-reducibility mechanism of titanium on maghemite catalysts for the SCR reaction: An in situ DRIFTS and quantitative kinetics study, Appl. Catal., B 221 (2018) 556–564.

[48] S. Xiong, J. Weng, Y. Liao, B. Li, S. Zou, Y. Geng, X. Xiao, N. Huang, S. Yang, Alkali metal deactivation on the low temperature selective catalytic reduction of NO_x with NH_3 over MnO_x-CeO_2: A mechanism study, J. Phys. Chem. C. 120 (2016) 15299–15309.

[49] B. Sun, Q. Li, G. Su, B. Meng, M. Wu, Q. Zhang, J. Meng, B. Shi, Insights into Chlorobenzene Catalytic Oxidation over Noble Metal Loading {001}-TiO_2: The Role of $NaBH_4$ and Subnanometer Ru Undergoing Stable $Ru^0 \leftrightarrow Ru^{4+}$ Circulation, Environ. Sci. Technol. 56 (2022) 16292–16302.

[50] Q. Wang, Y. Li, A. Serrano-Lotina, W. Han, R. Portela, R. Wang, M.A. Bañares, K. L. Yeung, Operando investigation of toluene oxidation over 1D Pt@CeO_2 derived from Pt cluster-containing MOF, J. Am. Chem. Soc. 143 (2021) 196–205.

[51] Y. Wang, H. Arandiyan, Y. Liu, Y. Liang, Y. Peng, S. Bartlett, H. Dai, S. Rostamnia, J. Li, Template-free Scalable Synthesis of Flower-like $Co_{3-x}Mn_xO_4$ Spinel Catalysts for Toluene Oxidation, Chemcatchem 10 (2018) 3429–3434.

[52] H. Sun, Z. Liu, S. Chen, X. Quan, The role of lattice oxygen on the activity and selectivity of the OMS-2 catalyst for the total oxidation of toluene, Chem. Eng. J. 270 (2015) 58–65.

[53] X. Wu, R. Han, Q. Liu, Y. Su, S. Lu, L. Yang, C. Song, N. Ji, D. Ma, X. Lu, A review of confined-structure catalysts in the catalytic oxidation of VOCs: synthesis, characterization, and applications, Catal. Sci. Technol. 11 (2021) 5374–5387.

[54] Y. Ryou, J. Lee, H. Lee, C.H. Kim, D.H. Kim, Low temperature NO adsorption over hydrothermally aged Pd/CeO_2 for cold start application, Catal. Today 307 (2018) 93–101.

[55] X. Yao, L. Zhang, L. Li, L. Liu, Y. Cao, X. Dong, F. Gao, Y. Deng, C. Tang, Z. Chen, L. Dong, Y. Chen, Investigation of the structure, acidity, and catalytic performance of CuO/$Ti_{0.95}Ce_{0.05}O_2$ catalyst for the selective catalytic reduction of NO by NH_3 at low temperature, Appl. Catal., B, 150- 151 (2014) 315–329.

[56] Y. Peng, J. Li, W. Si, X. Li, W. Shi, J. Luo, J. Fu, J. Crittenden, J. Hao, Ceria promotion on the potassium resistance of MnO_x/TiO_2 SCR catalysts: An experimental and DFT study, Chem. Eng. J. 269 (2015) 44–50.

[57] M.N. Khan, L. Han, P. Wang, J. He, B. Yang, T. Yan, L. Shi, D. Zhang, SO_2-tolerant NO_x reduction over ceria-based catalysts: Shielding effects of hollandite Mn-Ti oxides, Chem. Eng. J. 397 (2020), 125535.

[58] Q. Yan, S. Chen, C. Zhang, Q. Wang, B. Louis, Synthesis and catalytic performance of $Cu_1Mn_{0.5}Ti_{0.5}O_x$ mixed oxide as low-temperature NH_3-SCR catalyst with enhanced SO_2 resistance, Appl. Catal., B 238 (2018) 236–247.

[59] P. Lu, L. Ye, X. Yan, D. Chen, D. Chen, X. Chen, P. Fang, C. Cen, Performance of toluene oxidation over MnCe/HZSM-5 catalyst with the addition of NO and NH_3, Appl. Surf. Sci. 567 (2021), 150836.